Int. J. Electrochem. Sci., 16 **(2021)** Article ID: 210940, doi: 10.20964/2021.09.03

International Journal of ELECTROCHEMICAL SCIENCE
www.electrochemsci.org

Simulation and Experimental Verification of Buried Pipeline Corrosion under the High-Voltage Direct Current Interference

Shan Lin[1], *Xuehua Liu*[2], *Xianwei Zhang*[2], *Zhichao Cai*[2,*]

[1] Guangzhou Metro Design&Research Institute Co.,Ltd, Guangzhou 510010, China.
[2] School of Electrical and Automation Engineering, East China Jiaotong University, Nanchang 330013, China.
[*]E-mail: czchebut@foxmail.com

Received: 14 May 2021 / *Accepted:* 16 June 2021 / *Published:* 10 August 2021

Aimed at the corrosion caused by the ground current of the high-voltage direct current (HVDC) transmission system to adjacent buried pipelines, horizontal delamination is carried out according to different soil conductivities, and a field-circuit coupling model combining a resistor network model with an electric field model is established for the first time. The FEM model analyzed the distribution law of the grounding current in the soil, the change law of the ground and the pipeline potential, and the corrosion law of the buried pipeline caused by the ground current. Accurate judgment of the corrosion location of the buried pipeline and the quantitative calculation of the pipeline metal corrosion rate were all realized in the simulation. To verify the accuracy of the simulation, this paper develops an experimental platform on a small scale for the simulation model. The simulation and experimental results show results on the following fronts: a) under the influence of the HVDC grounding electrode ground current, the surface potential and pipeline potential cannot reflect the corrosion law of the buried pipeline; b) the corrosion location and corrosion degree of the buried pipeline mainly depends on the corrosion current density of the electrochemical reaction of the metal anode zone, and c) the different laying angles of the buried pipeline will change the corrosion location and trend of the pipeline metal.

Keywords: HVDC, finite element model, field-circuit coupling, corrosion experiment, buried pipeline

1. INTRODUCTION

In power transmission, a high-voltage direct current (HVDC) transmission system is widely used in the power transmission market based on its various advantages such as a large capacity, a high efficiency, and a long transmission distance [1-2]. However, in HVDC transmission systems, a large amount of current will flow into the earth through the grounding electrode and form a constant electric field in the soil, which will negatively affect the surrounding transmission lines, communication systems, buried pipelines and other facilities and even present safety risks to the operators [3-4].

At present, the main contents of the available research on grounding electrode ground currents include the influence of soil structure factors on the surface potential and pipeline potential [5-9] and the relationship between the surface potential or pipeline potential and the corrosion of buried pipelines [10-13]. Experiments have verified the relationship between soil resistivity, pH, salt content, leakage current density, and metal corrosion rate under the interference of grounding electrode currents [14-15]. In the process of studying the grounding electrode ground current, the specific calculation methods include the boundary element method, the finite element method, the moment method, and the traveling wave method [5,11,16-19]. The HVDC grounding electrode current running into the ground can be coupled with multiphysical fields with the help of simulation software, and the calculation result is closer to the actual situation [20-21], but applications in the study of the grounding current of HVDC rare at this stage. In addition, under the interference of the ground current of the DC grounding electrode, the traditional method to evaluate the corrosion degree of the pipeline is realized indirectly through changes in the surface potential and pipeline potential. Its accuracy needs to be verified, so there is an urgent need for a method that can accurately determine the corrosion area of buried pipelines and quantitatively calculate the corrosion degree.

Based on the above problems, field-circuit coupling of the resistance network model, the electric field model, and a pipeline corrosion model combining resistance and the finite element method are established for the first time. This paper selectively replaces good conductors such as grounding electrodes with resistance units and layers the soil horizontally according to the different electrical conductivities of the soil. The newly built model simulates and compares the surface potential, pipeline potential, and pipeline corrosion law under five groups of ground currents and three different pipeline burying modes. Finally, the simulation results are verified by the buried pipeline corrosion test, and the research results solve the problem of accurately identifying the pipeline corrosion area and calculating the pipeline corrosion depth, which provides a theoretical basis for the promotion and application of the finite element model in engineering.

2. GROUND CURRENT CORROSION MODELING THEORY

The unipolar ground loop operation mode is usually adopted in HVDC transmission projects in China at the initial stage of construction or under special circumstances, as shown in Fig. 1. The HVDC transmission system in Fig. 1 consists of three parts: a rectifier substation, a inverter station, and a DC transmission line. DC is transmitted from the rectifier station to the inverter station through the transmission line. In the process of current transmission, the current leaked to the earth by the grounding electrode of the inverter station will form an electric current field in the soil and eventually return it to the substation through the grounding electrode of the rectifier station.

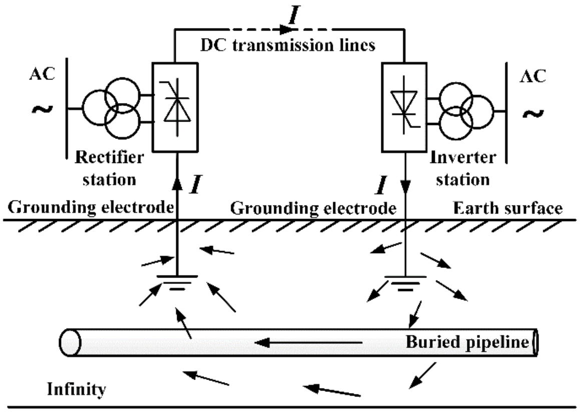

Figure 1. Schematic diagram of an HVDC ground electrode current entering the ground

2.1 Field-circuit coupling theory

The resistance network model performs equivalent calculations on grounding devices and uneven soil bodies to form a limited number of resistance loops. The mathematical model of the leakage current is established by the infinitesimal method, and an accurate curve of the leakage current distribution is obtained. Simple and convenient calculations are the advantages of the resistance network model, but there are also problems such as approximate calculations and large errors. The finite element electric field model does not approximate various parameters, and the error is small, so it can accurately simulate the current distribution law in the soil environment, but the current injected into the electric field does not have a reasonable source.

In this paper, the resistance network and electric field models are combined to form a field-circuit coupling model. This approach not only takes advantage of the simple and convenient calculation of the leakage current distribution of the resistance network model but also gives full play to the ability of the software simulation model to accurately simulate the distribution of the electric field and current in the soil environment. To avoid disturbance by ground factors, the pipeline is usually buried deep, which causes the conductivity of the soil layer near the pipeline to be very different from the conductivity of the upper soil layer near the ground. Soil processed under natural air drying has a typical horizontal layered structure of electrical conductivity, and the electrical conductivity of the upper soil is lower than that of the lower soil. The upper soil thickness d=3 m, the conductivity σ_1=0.02 S/m, and the lower soil conductivity σ_2=2 S/m [22], as shown in Fig. 2.

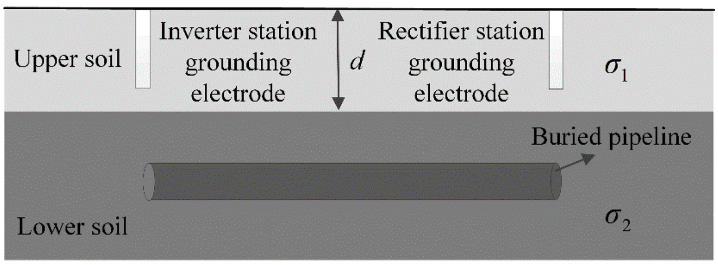

Figure 2. Schematic diagram of soil layering

This study establishes a field-circuit coupling model combining a circuit network and electric field according to Fig. 1, as shown in Fig. 3. The grounding electrode has a high electrical conductivity, which can be directly equivalent to resistance as a part of the circuit. The grounding electrode resistance of the inverter station and the rectifier station area respectively expressed by R_{j1} and R_{j2}. The surface resistance of the upper soil is represented by R_{d1}, and the lower surface soil is represented by R_{d2}. R_{d12} represents the transition resistance between the upper and lower soil surfaces.

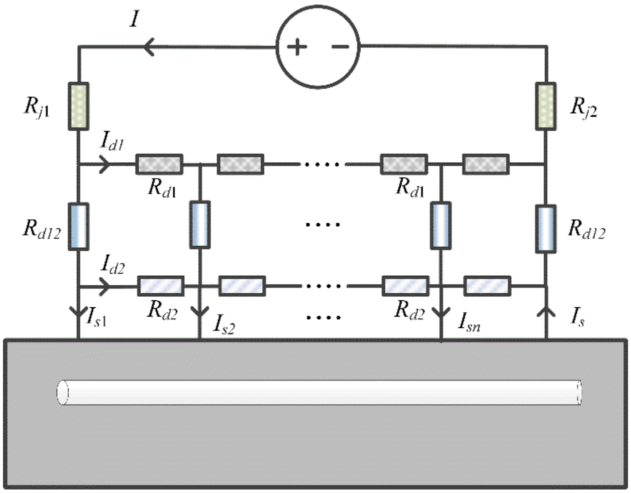

Figure 3. Field-circuit coupling model

The current of the HVDC transmission line is I, the current flowing into the surface of the upper soil is I_{d1}, and the current flowing into the surface of the lower soil is I_{d2}. According to Kirchhoff's current law, the stray current I_{s1} finally leaking into the lower soil can be expressed by equation (1):

$$I_{S1} = I - I_{d1} - I_{d2} \quad (1)$$

The return current I_S obtained by the infinitesimal method can be expressed by equation (2):

$$I_S = -\sum_{1}^{N} I_{SN} \quad (2)$$

Different from other DC interference sources, the HVDC grounding electrode has a unique current characteristic; the current amplitude varies greatly. When the system is operating in a unipolar earth loop, the ground current of the grounding electrode can reach several thousand amperes [5].

According to the fluctuation of the load of the HVDC transmission line, the injection current generated by the ground current in the pipeline is shown in Fig. 4. The injection current $I_{SN/2}$ of the middle position of the buried pipeline under different ground currents is 1 A, 2 A, 3 A, 4 A, and 5 A. These five groups of current data are selected as the finite element electric field model to simulate the injection current.

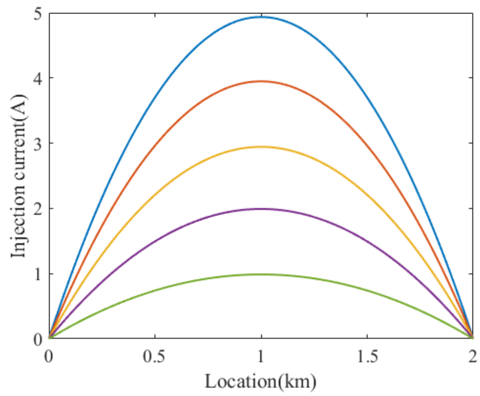

Figure 4. Injection current acting on the buried pipeline

2.2 Theory of current distribution into ground

The soil in the same horizontal layer is considered to be a uniform conductive material, so the electric field applied to the soil area should follow the law of conservation of current and Ohm's law:

$$\nabla \cdot \boldsymbol{i} = 0 \tag{3}$$

$$\boldsymbol{i} = -\sigma \nabla \varphi \tag{4}$$

where ***i*** represents the current vector density, σ and φ are the conductivity and potential of the electrolyte, respectively.

2.3 Electrochemical corrosion theory

The ground current of the grounding electrode will flow through the buried pipeline. This part of the current will promote the electrochemical reaction generated by the buried pipeline. It contains two parts:

Iron oxidation reaction: $Fe \rightarrow Fe^{2+} + 2e^-$ (anode)

Oxygen reduction reaction: $O_2 + 2H_2O + 4e^- \rightarrow 4OH^-$ (cathode)

Oxygen is an important factor in the electrochemical reaction, and the speed of electrochemical corrosion is related to oxygen concentration. The diffusion of oxygen in the soil satisfies Fick's law:

$$\nabla \cdot D_{O_2}\left(\nabla C_{O_2}\right) = 0 \tag{5}$$

The speed of pipeline metal corrosion depends on the current density involved in buried pipeline corrosion, namely, the corrosion current i_{Fe}. The corrosion current i_{Fe} can be controlled by the Tafel dynamic equation [20]:

$$i_{Fe} = \left(\frac{c}{c_{ref}}\right) i_{0,Fe} 10^{\frac{\eta_{Fe}}{A_{Fe}}} \tag{6}$$

$$i_{O_2} = \left(\frac{c}{c_{ref}}\right) i_{0,O_2} 10^{\frac{\eta_{O_2}}{A_{O_2}}} \tag{7}$$

where C_{ref} is the oxygen concentration of the pipe-soil surface, $i_{0,Fe}$, $i_{0,O2}$ is the oxygen exchange current density of the anode and cathode reactions, and A_{o2} and A_{Fe} are the Tafel slopes. The overpotential is calculated according to the following expression:

$$\eta = \varphi_S - \varphi_l - E_{eq,m} \tag{8}$$

where φ_S is the electrode potential, φ_l is the electrolyte potential, and $E_{eq,m}$ is the equilibrium potential of the electrode reaction. According to Faraday's law, the corrosion rate of buried pipes (iron) can be expressed by the rate at which the metal loses electrons:

$$v_{loss} = \frac{M}{nF} i_{Fe} \tag{9}$$

where M is the average molar mass of iron; n is the number of electrons lost in the iron reaction; and F is the Faraday constant. The unit of v_{loss} is g/(m^2·h). The corrosion depth is also used in engineering applications to indicate the corrosion rate of metals. The corrosion depth refers to the thickness of the metal that is corroded in unit time, expressed in v_{depth}, which is:

$$v_{depth}\left(mm/h\right) = \Delta d / t \tag{10}$$

where Δd is the thickness of metal corrosion, in mm, and t is the corrosion time. When the corrosion time t is in years, the metal corrosion rate formula is:

$$v_{depth}\left(mm/a\right) = 365 \times 24 \Delta d / t \tag{11}$$

The quality index of the metal corrosion rate can be converted between v_{loss} (g/(m ·h)) and v_{depth} (mm/a). The conversion formula is as follows [23]:

$$v_{depth}\left(mm/a\right) = 8.76 v_{loss} / \rho \tag{12}$$

where 8.76 is the unit conversion factor.

3. FINITE ELEMENT SIMULATION ANALYSIS

3.1 Modeling

The three-dimensional hemispherical resistance network model [24] and multilayer different conductivity model [25] are common resistance network models. The resistance network model is simple and easy to calculate, but there are many idealized assumptions, which are difficult to use in all practical situations [26], so this article introduces finite element simulation analysis. In this paper, a dynamic three-dimensional finite element model, which distinguishes and separates the modeling of buried pipelines, including a grounding electrode, a buried pipeline, and a soil domain, is established [27-29].

Full-size simulation analysis is more difficult in actual engineering practice [30]. To facilitate experimental verification and calculation, a reduced-size grounding electrode is used to construct the geometric structure of the buried pipeline that is corroded by the ground current through finite element software, as shown in Fig. 5, where the dimensions of the soil area are 400 mm × 240 mm × 150 mm, the grounding electrode length is 50 mm, and the diameter is 8 mm. The distance is 120 mm in the length direction of the soil and 20 mm in the width direction. The upper surface of the grounding electrode coincides with the soil surface, and the distance between the two grounding electrodes is 360 mm.

Suppose ground electrode 1 (inverter station) is the inflow end of the ground current and ground electrode 2 (rectifier station) is the outflow end of the ground current. Between the two grounding electrodes, a buried pipeline with an inner diameter of 10 mm, an outer diameter of 15 mm, and a length of 200 mm is laid at a distance of 30 mm from the ground surface.

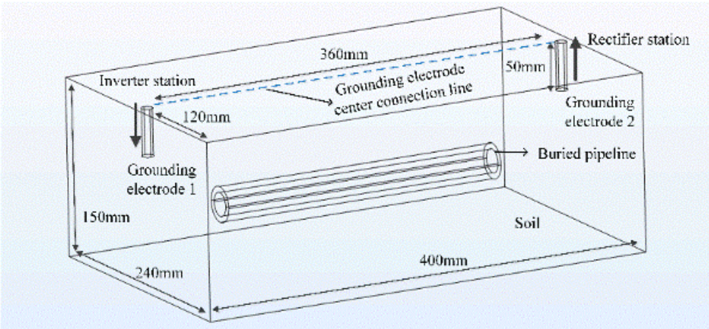

Figure 5. Model geometry and size

Fig. 6 shows the geometric structure mesh division diagram when the buried pipeline is parallel (0°) to the central connection line of the grounding electrode, and the mesh is divided by tetrahedral elements. Tetrahedral elements are also used to divide the mesh of the model structure when buried pipelines placed at 45° and vertical (90°) intersect at the centerline of the grounding electrode.

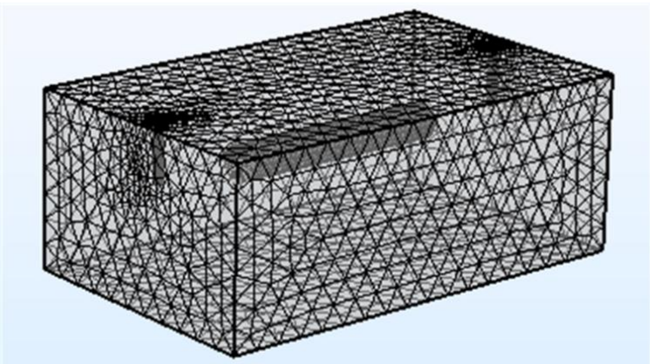

Figure 6. Schematic diagram of meshing

Table 1. Parameters of the simulation model

Parameter	Value	Unit	Description
$E_{eq,Fe}$	-0.76	V	Equilibrium potential of iron
$E_{eq,O2}$	1.23	V	Equilibrium potential of oxygen
$i_{0,Fe}$	7.1E-5	A/m^2	Iron exchange current density
$i_{0,O2}$	1E-8	A/m^2	Oxygen exchange current density
A_{Fe}	0.41	mV/dec	Iron ion reduction Tafel slope
A_{O2}	-0.25	mV/dec	Oxygen ion reduction Tafel slope
D_{O2}	1E-7	m^2/s	Oxygen diffusion coefficient
C_{O2}	0.2	mol/m^3	Initial oxygen ion concentration

M	56	g/mol	The average molar mass of iron
n	2	1	Loss of iron electrons
σ_{Fe}	1E7	S/m	Pipeline metal conductivity
σ_l	2	S/m	Soil conductivity
F	96485	C/mol	Faraday's constant

In the modeling process, the soil, grounding electrode, buried pipeline material, and related boundary conditions in the model are assigned according to the corresponding parameters in Table 1 [31-32]. In practical engineering, different laying methods of buried pipelines will affect the transmission line [33]. Five groups of simulation analyses are carried out in the simulation models of three different pipeline laying modes, in which the injection currents are 1A, 2A, 3A, 4A, and 5A. At the same time, the distribution of current density, surface potential, and pipeline potential was analyzed [34].

3.2 Current density distribution

Fig. 7 is a cloud diagram of the current density distribution in the solution domain under the same boundary conditions (injected currents are all 2 A) for the three pipeline laying methods. The comparison shows that the overall flow direction of the current in the soil is consistent and results from grounding electrode 1 (inverter station grounding electrode) and run to grounding electrode 2 (rectifier station grounding electrode). However, due to the different laying angles of buried pipelines, the current density flowing through the pipelines changes. The buried pipeline laid parallel (0°) to the center connection line of the two grounding electrodes has the darkest color; that is, the current density flowing through the pipeline is the largest, followed by those placed 45° and vertical (90°) to the center connecting line of the grounding pole buried pipeline

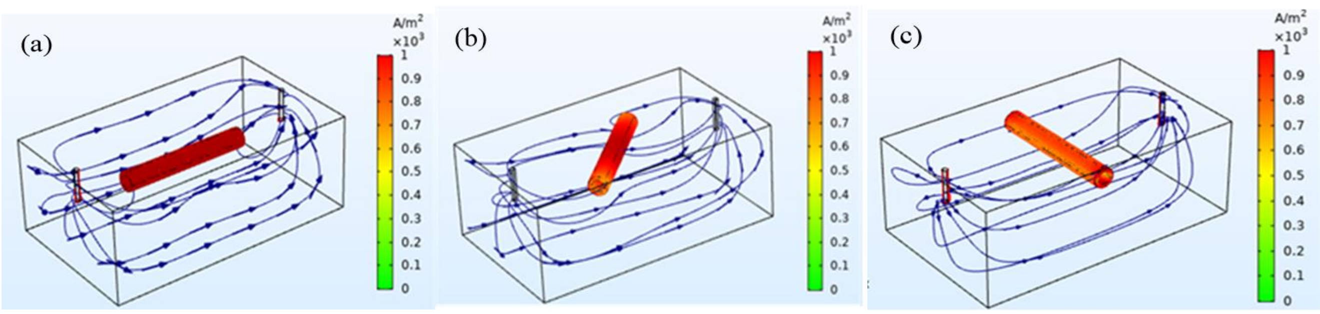

Figure 7. Current density distribution cloud chart: (a) parallel (0°) arrangement, (b) 45° arrangement, and (c) vertical (90°) arrangement

3.3 Surface potential distribution

Fig. 8 shows the surface potential curve on the central connecting line of the two grounding electrodes under the action of the current. It can be seen from the diagram that the overall distribution trend of the surface potential under the action of five groups of currents (1A-5A) remains consistent.

The surface potential at grounding electrode 1 is the largest, and the potential at grounding electrode 2 is 0 V. In general, the ground surface potential shows a downward trend along the central connection line of the two electrodes. The ground surface potential drops at a higher rate near the two grounding electrodes (0.024-0.1 m and 0.3-0.36 m), and the middle part (0.1-0.3 m) is relatively flat. The surface potential is positively correlated with the injected current; the greater the injected current is, the greater the surface potential.

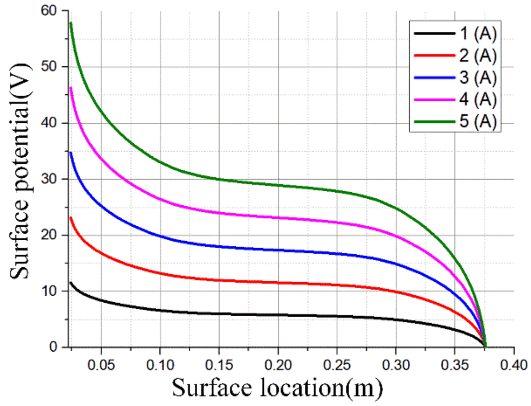

Figure 8. Curve of surface potential distribution between the two grounding electrodes

3.4 Pipeline potential distribution

Figs. 9 shows the potential of the centerline along the length direction of the upper surface of the buried pipeline from three different angles. The greater the injected current (1A to 5A) is, the greater the pipeline potential. As shown in Fig. 9a and 9b, the potential along the pipeline gradually decreases from grounding electrode 1 to grounding electrode 2. Fig. 9c shows that the potential at the middle position of the buried pipeline is the highest, and the potential at both ends of the pipeline is the lowest. However, in general, because buried pipe metal is a good conductor, the pipeline potential on the same pipeline has little difference.

Under the action of the same injection current, compared with different laying angles, the angles of pipeline potential from large to small are 45°, 90°, and 0°.

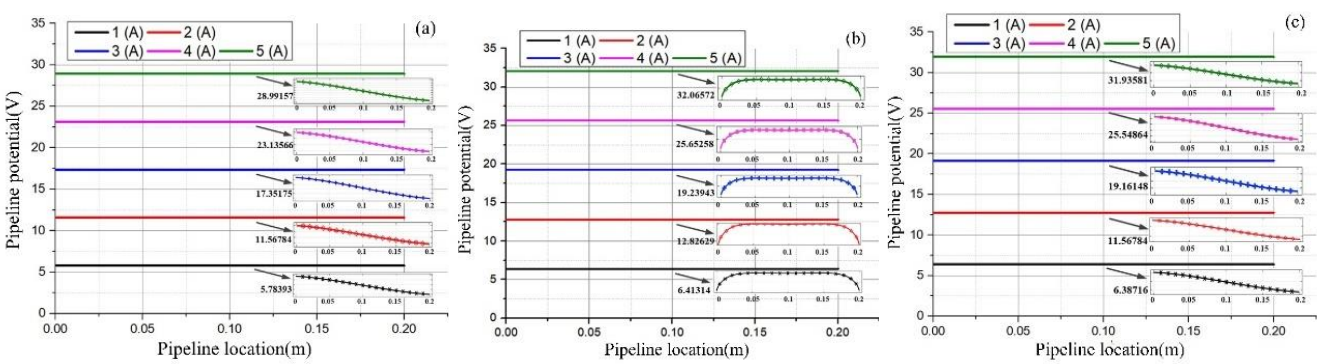

Figure 9. Potential distribution curve of the buried pipeline: (a) parallel (0°) arrangement, (b) 45° arrangement, and (c) vertical (90°) arrangement

According to the traditional method of indirectly evaluating the corrosion tendency of buried pipelines based on surface potential and pipeline potential, the corrosion of pipelines should be greater in positions with higher surface and pipeline potentials [35]. According to the trend of surface potential analysis in Fig. 8, the surface potential near grounding electrode 1 is the largest, so the pipeline closer to grounding electrode 1 is more severely corroded. According to the potential distribution trend of the pipeline in Figs. 9, the potential along the same buried pipeline does not change much, so the corrosion trend of the pipeline should be approximately the same. There are different conclusions available to indirectly evaluate the trend of pipeline corrosion from the point of view of surface potential and pipeline potential, which are obviously not consistent with reality.

3.5 Corrosion current density distribution

To solve the above problems, electrochemical corrosion theory is introduced. The essence of the corrosion of buried pipeline metal is electrochemical corrosion [36]. Corrosion occurs in the anode area of the metal, namely, the area where the metal loses electrons (the outflow area of the corrosion current), while the cathode area of the metal, namely, the area where the corrosion current flows into, does not lose electrons, and the metal will not be corroded.

Finite element software can realize the coupling calculation of the "constant electric field" module and "electrochemistry" module. In three different layout models of buried pipelines, the coupling calculation of the model is carried out based on five groups of different injection currents (1A to 5A). According to equation (6), the calculation step length is set to 0, 0.1, and 72 h. The corrosion current density cloud diagrams on the three groups of pipes shown in Figs. 10 can be obtained by simulation, and the current density curve on the specified straight line on the pipeline can be drawn. The blue part of the cloud image is the area where the current flows into the pipeline, and the corresponding current density curve value is positive, indicating the cathodic reaction area of the pipeline, and the pipeline does not produce corrosion. The red part of the cloud image is the area where the current flows out of the pipeline, and the corresponding current density curve value is negative, indicating the anodic reaction area of the pipeline, that is, the corrosion area of the pipeline.

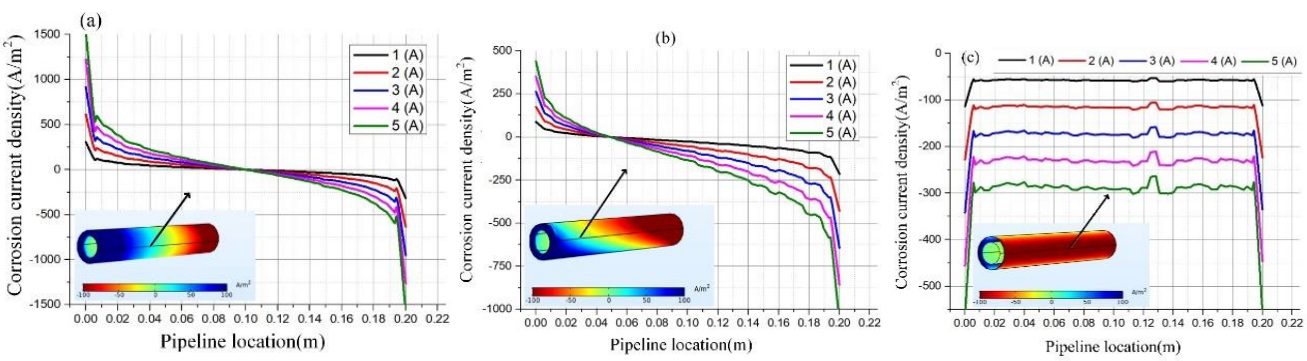

Figure 10. Corrosion current density distribution on the buried pipelines: (a) parallel (0°) arrangement, (b) 45° arrangement, and (c) vertical (90°) arrangement

When arranged in parallel (0°), the positive and negative current density areas of the buried pipeline are symmetrically distributed, that is, the corrosion is uniform. When arranged at 45°, the negative current density area of the buried pipeline increases, that is, the corrosion area increases. In the vertical arrangement (90°), the collection line covers all negative current density areas, that is, the whole surface is corroded; the other side of the pipeline corresponding to the collection line is the location at which the external current flows into the pipeline, so there is almost no corrosion. Comparative analysis can be obtained; the corrosion area and corrosion current density of the pipeline are obviously different with different pipeline laying methods. Three groups of corrosion test experimental platforms were built below and verified by experiments to verify the accuracy of the above simulation results.

4. EXPERIMENTAL VERIFICATION

4.1 Experimental

To verify the accuracy of the finite element model simulation, the corrosion platform of the buried pipeline (in equal proportion to the simulation model) was built, as shown in Figs. 11. Compared with the sleeper specimen corrosion experiment [37], the extra electrode double reaction cell experiment [38], and the impressed current interference experiment [39], this experiment does not need to use an electrochemical workstation, the experimental equipment is simple, and the difficulty of the experiment can be reduced. The injection current is applied by the programmable DC power supply, and the current value is set to 2 A. Five hundred grams of sodium chloride, 300 g of sodium bicarbonate, and 100 g of sodium sulfate are dissolved in 0.4 m × 0.24 m × 0.15 m of distilled water [40], and a solution to simulate the corrosive soil environment was configured with an electrical conductivity of 2 S/m (consistent with the electrical conductivity of the soil in the simulation model). The material of the buried pipe specimen is 20# carbon steel, and its diameter and length are consistent with the simulation model. The two grounding electrodes are replaced by two carbon rods. The analog simulation model is used to conduct corrosion experiments on three groups of pipelines with different laying methods (0°, 45°, and 90°). The injection current is 2 A. After 72 h of electrification, the experimental and simulation results are observed.

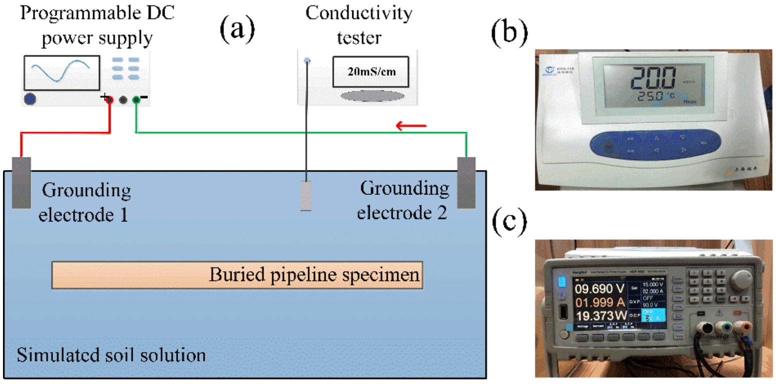

Figure 11. Buried pipeline corrosion test platform

4.2 Comparison of corrosion morphology between experiment and simulation

The experimental and simulated corrosion morphologies under the same conditions are generally consistent, as shown in Figs. 12. The corrosion experiment of the buried pipeline reflects the corrosion speed through the corrosion depth of the pipeline, while the simulation model uses the rate at which the metal loses electrons, that is, the corrosion rate, to characterize the corrosion speed. Equation (12) is used to convert the simulated corrosion rate into the corrosion depth and compare it with the experimental results to verify the consistency of the corrosion test and simulation results [41].

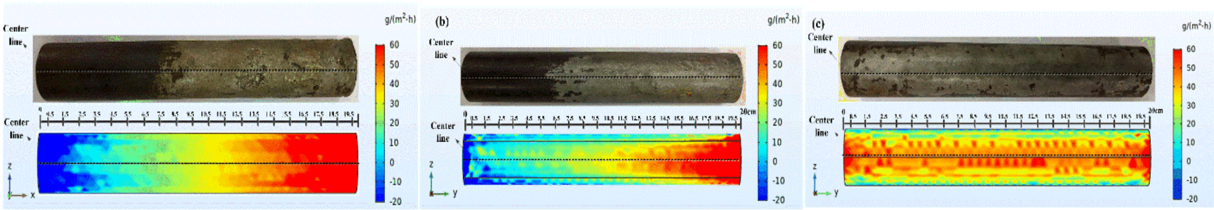

Figure 12. Comparison of simulation and experimental corrosion morphology: (a) parallel (0°) arrangement, (b) 45° arrangement and (c) vertical (90°) arrangement

4.3 Thickness measurement process

The pipeline corrosion thickness was measured by the RAM-5000 SNAP general-purpose computer-controlled nonlinear ultrasonic detection system developed by RITEC Company in the United States. The thickness measurement process is shown in Figs. 13.

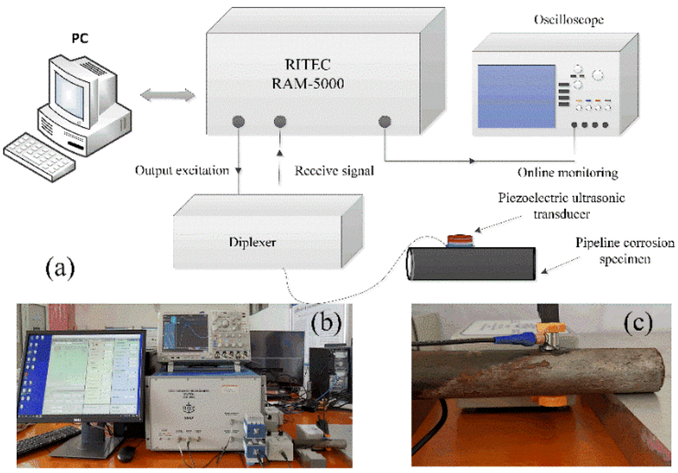

Figure 13. Block diagram of the thickness measurement system and physical diagram of the thickness measurement process: (a) block diagram of the thickness measurement system, (b) test device and (c) pipeline specimen

The ultrasonic longitudinal wave resonant thickness measurement method is used to measure the thickness of the tube wall. The principle is that when the thickness of the test tube wall is an integer multiple of the ultrasonic wavelength, the incident wave and reflected wave excited by the electromagnetic ultrasonic transducer will resonate inside the tube wall [42]. Under broadband incentives, multiple resonance frequencies will be obtained, and the first resonance frequency f_m and resonance interval Δf can be represented as:

$$f_m = m\frac{v}{2\Delta d} \tag{13}$$

$$\Delta f = f_m - f_{m-1} = \frac{v}{2\Delta d} \tag{14}$$

where v is the propagation velocity of a longitudinal wave through the specimen, which is related to the properties of the tested material [43]. The propagation velocity of a longitudinal wave in the buried pipeline specimen of 20# carbon steel is approximately 5900 m/s. Δd is the thickness of the test specimen. The thicknesses of 20 points (0.5 cm, 1.5 cm, 2.5 cm, ... 19.5 cm) corresponding to the three groups of buried pipelines with different arrangements in Figs. 12 were measured. For places where the surface of the specimen is too rough, it is treated with sandpaper before thickness measurement.

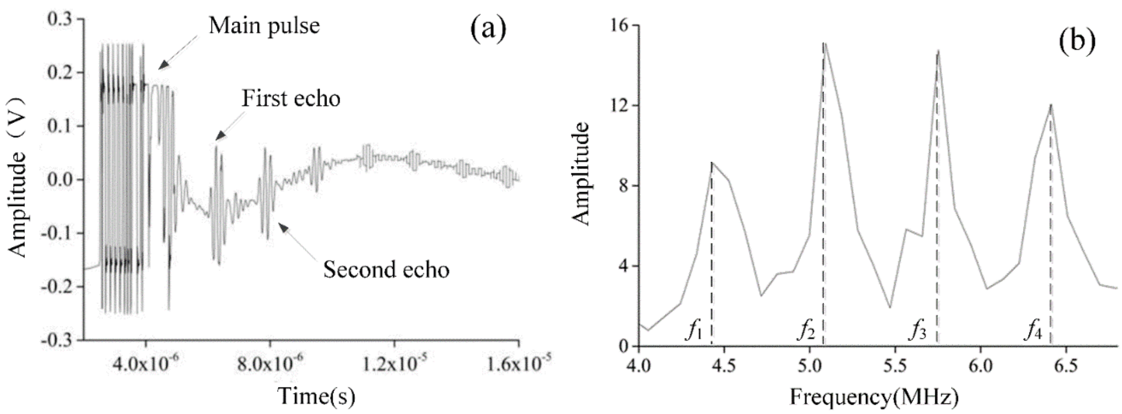

Figure 14. Time domain diagram and spectrogram of the excitation echo signal: (a) time domain diagram and (b) spectrum diagram

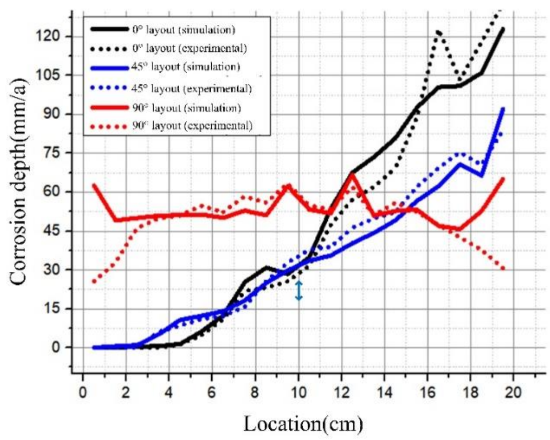

Figure 15. Corrosion depth comparison curve between pipeline simulation and experiment

Fig. 14a shows the separation of longitudinal waves in the time domain generated by pulse excitation excited by the measurement system. Fig. 14b is the frequency spectrum obtained by Fourier transform, and the resonant frequency can be obtained. According to equation (14), the thickness of the buried pipeline specimen after corrosion can be calculated.

4.4 Comparison of corrosion depth between simulation and experiment

The corrosion loss thickness data of the experimental pipeline and the corrosion rate data of the pipeline obtained from the finite element simulation were statistically analyzed, as shown in Table 2. The two sets of data were converted into corrosion depth (mm/a) by equation (11) and equation (12) and plotted as shown in Fig. 15.

Table 2. Parameters of simulation model

θ	0°	45°	90°	0°	45°	90°
Location (cm)	Simulation: Corrosion rate (g/m2·h)			Corrosion Thickness(mm)		
0.5	0	0	55.68	0	0	0.21
1.5	0	0.48	43.74	0	0	0.27
2.5	0.35	0.87	44.53	0	0	0.38
3.5	0.53	4.55	45.35	0	0.05	0.41
4.5	1.27	9.53	45.56	0.01	0.07	0.42
5.5	5.62	10.93	45.75	0.04	0.09	0.45
6.5	11.04	12.53	44.61	0.09	0.1	0.43
7.5	22.51	16.19	47.08	0.18	0.13	0.48
8.5	27.48	22.24	45.52	0.19	0.21	0.46
9.5	25.29	26.52	55.5	0.21	0.27	0.52
10.5	31.06	29.89	47.43	0.26	0.31	0.45
11.5	47.87	31.65	46.21	0.39	0.32	0.44
12.5	60.14	35.87	59.36	0.47	0.38	0.51
13.5	65.51	39.43	45.37	0.51	0.41	0.42
14.5	71.73	43.73	46.98	0.57	0.43	0.46
15.5	82.51	50.45	47.41	0.73	0.51	0.43
16.5	89.52	5.48	41.86	1.01	0.57	0.39
17.5	89.92	62.91	40.73	0.85	0.62	0.35
18.5	94.43	59.09	46.91	0.97	0.58	0.31
19.5	109.52	82.08	57.97	1.09	0.69	0.25

Fig. 15 shows that the corrosion depth rise rate is largest when arranged in parallel (0°). The closer to the right end of the pipeline the simulation is, the greater the corrosion depth. The maximum error of the simulation and experiment occurs at 17.5 cm along the pipeline. The annual corrosion error is 16.6%, and the error rates of other positions are less than 10%. When arranged at 45°, the corrosion depth of the simulation and experiment corresponding to each collection point also showed an upward trend from the left end to the right end of the pipeline, but the ascending rate was not as high as at 0°. The maximum error of the corrosion depth between the simulation and experiment appeared at 12.5 cm. In the vertical arrangement (90°), the maximum corrosion depth error of the simulation and experiment occurs at both ends of the pipeline (0.5 cm and 19.5 cm), and the corrosion depth curve and size of the middle part of the pipeline from 1.5 cm to 18.5 cm are almost the same. The comparative experiment and simulation results show that the finite element simulation model is feasible for predicting the corrosion location and corrosion depth of buried pipelines.

5. CONCLUSION

This paper studies the corrosion of the ground current of the grounding electrode to the adjacent buried pipeline in an HVDC system under the unipolar ground loop operation mode. Through simulation results and experimental verification, the following conclusions are obtained:

1) A field-circuit coupling model combining the resistor network model with the electric field model was established for the first time by layering the soil horizontally according to different conductivities. The corrosion of buried pipelines with five sets of injection currents under three different laying modes is simulated and analyzed. The injected current directly affects the surface potential near the grounding electrode and the pipeline potential; the ground surface potential between the two grounding electrodes shows a downward trend from the ground electrode of the inverter station to the ground electrode of the rectifier station. Under the same injection current, the maximum absolute value of the pipeline potential change does not exceed 1.5×10^{-5} V.

2) The corrosion area of the buried pipeline can be located directly, and the corrosion rate can be calculated by electrochemical corrosion simulation analysis of a three-dimensional finite element model. When the injection current is 2 A, the maximum corrosion rate in the simulation when the pipeline is arranged at 0° and 45° appears near the grounding electrode of the rectifier station; when the pipeline is arranged at 90°, the corrosion rate at each position of the pipeline is relatively uniform. An experimental platform that is proportional to the simulation model is built for verification. When the injection current is 2 A, the maximum corrosion thickness of the pipeline in the 0° and 45° arrangements in the experiment appears near the grounding electrode of the rectifier station; when the pipeline is arranged at 90°, the corrosion thickness at each position of the pipeline is relatively uniform. After formula conversion, the simulation data and experimental data are in good agreement; that is, the experiment can verify the accuracy of the simulation.

3) The maximum corrosion rate is analyzed under different laying methods, and the corrosion protection of buried pipelines near the grounding electrode of the rectifier station is strengthened to avoid major accidents. Therefore, the finite element corrosion model can guide the laying and protection of buried pipelines in engineering applications.

ACKNOWLEDGMENT
This work was supported in part by the Natural Science Foundation of China under Grant 51807065, in part by the Key Research and Development Plan of Jiangxi Province under Grant 20202BBEL53015.

CONFLICTS OF INTEREST
The authors declare no conflict of interest.

References

1. H. Zhang, Y.X. Du, R.Z. Qin and Z.T. Jiang, *Corros. Prot.*, 41 (2020) 40.
2. L. Zhang, M. He, L. and F. Zhang, *Nat. Gas Ind.*, 39 (2019) 134.
3. C.F. Gao, Q.L. Gu, Y.T. Jiang, Y.F. Li, J. Mao, L.R. Xiu, X.Y. Wang and Z.T. Jiang, *Nat. Gas Ind. B*, 6 (2019) 427.
4. J.L. Li, C.C. Jia and P. Feng, *Isulat. Surge Arrest.*, 294 (2020) 1.
5. X.B. Meng, B. Zhang, Y.L. Liao, R.H. Li, B. Gong and F.Y. Cao, *Proc. CSEE,* 631 (2019) 6113.
6. P.J. Lagace, J.L. Houle, Y. Gervais, D. Mukhedkar, *IEEE Trans. Power Delivery*, 3 (1988) 1573.
7. C.E. Caroli, N. Santos, D. Kovarsky, M.A.M. Marques, *IEEE Trans. Power Delivery*, 3 (1988) 1211.
8. B. Zhang, R. Zeng, J. He, J. Zhao, X. Li, Q. Wang and X. Cui, *IET Gener. Transm. Distrib.*, 2 (2008) 185.
9. J.E.T. Villas and C.M. Portela, *IEEE Trans. Power Delivery*, 18 (2003) 867.
10. J.M. Lu, D. Xiao, C.X. Mao and G.H. Mei, *High Voltage Eng.*, 09 (2006) 55.
11. S.Y. Zhu, T. Yuan and B. Xu, *Power Syst. Technol.*, 38 (2014) 2304.
12. Z.B. Yu, L.G. Liu, Z.Z. Wang, M. Li and X.L. Wang, *IEEE Trans. Appl. Supercond*, 29 (2019) 1.
13. C. LÜ, Y.X. Zhang, Y.F. Li, X.Y. Wang and Z.T. Jiang, *Corros. Prot.*, 41 (2020) 43.
14. T. Gu, F. Bai, C. Yu, J.Z. Li, Y. Wang and F.Y. Cao, *Corros. Prot.*, 40 (2019) 902.
15. X.F Tong, Z.H. Zheng, B. Tan, H.L. Lu and X.S. Wen, *IEEE Access*, 06 (2018) 57230.
16. Q. Xiong, M.X. Wang, Huang Hao, Y. Shi and H.T. Tang, *Proc. CSEE*, 40 (2020) 2269.
17. Y. Si, Z.Z. Wang, L.G. Liu, H.M. Li and W.G. Zhao, *Trans. China Electron. Soc.,* 35 (2020) 4448.
18. Y. Hong, Z.H. Li, G.F. Qiao and J.P. Ou, *Constr. Build. Mater.*, 157 (2017) 416.
19. T. Yuan, T.X. Li, W.X. Sima, S.W. Liu, D.H. Luo and X.C. Li, *Proc. CSEE*, 38 (2018) 5266.
20. Z.C. Cai, X.W. Zhang, H. Cheng, *IEEE Access*, 07 (2019) 168404.
21. Z.Z, Zhao, Y.K. Wang, Y.H. Li, J.X. Song and G.Q. Liu, *High Voltage Appar.*, 56 (2020) 62.
22. G. Wen, S.J. Qi, Q.B. Jiang and X.H. Cai, *Trans. China Electron. Soc.,* 31 (2016) 91.
23. J.L. Li, Y.B. Li, K. Xu, L.Y. Guo and P.W. He, *High Voltage Appar.*, 44 (2018) 1572.
24. H.W.M. Smulders and M.F.P. Janssen, Proceedings of the 7th World Congress on Railway Research, Montréal, Canada, 2006.
25. A. Zaboli, B. Vahidi, S. Yousefi and M.M. Hosseini-Biyouki, *IEEE Trans. Veh. Technol.*, 66 (2016) 974.
26. Z.C. Cai and X.W. Zhang, *J. East China Jiaotong Univ.*, 33 (2020) 27.
27. X.H. Wang, C. Xu, Q. Liu, C.Y. Tu, Y.C. Chen and Y.C. Li, *Int. J. Electrochem. Sci.*, 12 (2017) 6520.
28. J.H. Hu, Z.F. Tang, F.Z. Lv, X.H. Pan. Y. Han and X.Y. Jiang, *J. Zhejiang Univ. (Eng. Sci.)*, 49 (2015) 116.
29. Y. Sun, Y. Yuan and Chao Lv, *J. Xuzhou Inst. Technol. (Nat. Sci. Ed.)*, 35 (2020) 48.
30. H. Jin and S. Yu, *Constr. Build. Mater.*, 272 (2021) 121646.
31. G. Doyle, M. V Seica, and M.W.F. Grabinsky, *Can. Geotech. J.*, 40 (2003) 225.
32. R.N. Deo, N. Birbilis, and J.P. Cull, *Corros. Sci.*, 80 (2014) 339.
33. P.F. Zhang and X.C. Yu, *Corros. Prot.*, 32 (2011) 146.
34. P. Peng. X.J. Zen. Y.R. Ni. K. Yu. Y. Leng. W.H. Zhou and Y.H. Xie, J. Electr. *Power Sci. Technol.*, 36 (2021) 192.
35. T. T.Duignan, *J. Colloid Interface Sci.*, 600 (2021) 338.
36. X.H. Wang, X.T. Song, Y.C. Chen and Z.Q. Wang, *Int. J. Electrochem. Sci.*, 13 (2018) 5654.
37. J.L. Li, Y.B. Li, K. Xu, L.Y. Guo and P.W. He, *High Voltage Appar.*, 44 (2018) 1572.
38. X.B.E Su, W.W. Wang, L. Wang and H. Yu, *Int. J. Electrochem. Sci.*, 15 (2020) 2261.
39. Y. Yang, M. Sun, Y.L. Luo, W.G. Zeng and R.Y. He, *Int. J. Electrochem. Sci.*, 16 (2021) 150927.
40. K.K. *Tang, Cem. Concr. Compos.*, 109 (2020) 103552.
41. Z.H. Wang, Z.F. Zhang and R.R. Li, *Henan Sci.*, 38 (2020)1742.

42. G.C. Davis, *J. Nutr*., 125 (2021) 1.
43. Z.Z Zhang, Y.H. Dan, J. Zou, G.H. Liu, C.F. Gao and Y.Q. Li, *IEEE Access*, 07 (2019) 59287.